Chapter 9
Towards Computing High-Order p-Harmonic Descent Directions and Their Limits in Shape Optimization

Henrik Wyschka, Martin Siebenborn

Abstract We present an extension of an algorithm for the classical scalar p-Laplace Dirichlet problem to the vector-valued p-Laplacian with mixed boundary conditions in order to solve problems occurring in shape optimization using a p-harmonic approach. The main advantage of the proposed method is that no iteration over the order p is required and thus allows the efficient computation of solutions for higher orders. We show that the required number of Newton iterations remains polynomial with respect to the number of grid points and validate the results by numerical experiments considering the deformation of shapes. Further, we discuss challenges arising when considering the limit of these problems from an analytical and numerical perspective, especially with respect to a change of sign in the source term.

9.1 Introduction

Shape optimization constrained by partial differential equations is a vivid field of research with high relevance for industrial grade applications. Mathematically, we consider the problem

$$\begin{aligned} \min_{\Omega \in \mathscr{A}} \quad & J(v_s, \Omega) \\ \text{s.t.} \quad & \mathscr{E}(v_s, \Omega) = 0 \end{aligned}$$

where J denotes the objective or shape functional depending on a state variable v_s and a Lipschitz domain $\Omega \subset \mathbb{R}^d$, which is to be minimized over the set of admissible shapes $\mathscr{A}$. Further, the state and the domain have to fulfill a PDE constraint $\mathscr{E}$. A

Henrik Wyschka
Department of Mathematics, Universität Hamburg, Germany
e-mail: henrik.wyschka@uni-hamburg.de

Martin Siebenborn
Department of Mathematics, Universität Hamburg, Germany
e-mail: martin.siebenborn@uni-hamburg.de

A. Iske, T. Rung (eds.), *Modeling, Simulation and Optimization of Fluid Dynamic Applications*, Lecture Notes in Computational Science and Engineering 148,
https://doi.org/10.1007/978-3-031-45158-4_9

common solution technique for this type of problem is to formulate it as a sequence of deformations to the initial shape [18]. Each of these transformations has the form

$$\tilde{\Omega} = (\mathrm{id} + tv)(\Omega) \tag{9.1}$$

for a step-size $0 < t \leq 1$ and a descent vector field $v : \mathbb{R}^d \to \mathbb{R}^d$ in the sense $J'(\Omega)v < 0$ with shape derivative denoted by J'. Hence, the set $\mathscr{A}$ is implicitly defined by all shapes reachable via such transformations to the initial shape. From the analytical derivation of this procedure it is required that the v are at least $W^{1,\infty}(\mathbb{R}^d, \mathbb{R}^d)$ inherently ensuring that all admissible shapes remain Lipschitz. However, in practice this condition is often neglected and so-called Hilbert space methods [1] are used. The most prominent example of those consists of finding $v \in W^{k,2}(\Omega, \mathbb{R}^d)$ for some $k \in \mathbb{N}$. This results in smooth shapes, which are relevant for some applications, but are not necessarily optimal. Further, the mesh quality often deteriorates and it would require a high differentiability order k to obtain a Lipschitz transformation from the Sobolev embedding.

Recent development suggests using a p-harmonic approach [3] to determine descent directions. This technique can be obtained by considering the steepest descent in the space of Lipschitz transformations

$$\underset{\substack{v \in W^{1,\infty}(\Omega, \mathbb{R}^d) \\ \|\nabla v\|_{L^\infty} \leq 1}}{\arg\min} \quad J'(\Omega)v. \tag{9.2}$$

and then potentially relax the problem. The descent field is obtained by the solution of a minimization problem for $2 \leq p < \infty$ reading

$$\underset{v \in W^{1,p}(\Omega, \mathbb{R}^d)}{\arg\min} \frac{1}{p} \int_\Omega \|\nabla v\|_2^p \, \mathrm{d}x + J'(\Omega)v. \tag{9.3}$$

Since the classical Hilbert space setting is recovered for the linear case $p = 2$, this approach can also be understood as a regularization of such methods. It is demonstrated that this approach is superior in terms of representation of sharp corners as well as the overall mesh quality and yields improving results for increasing p [12]. On the downside, the stated numerical examples also made clear that it is challenging to compute solutions for $p > 5$ due to serious difficulties in numerical accuracy and the need to iterate over increasing p with the presented solution technique.

We now assume that the shape derivative $J'(\Omega)$ can be expressed via integrals over the domain and the boundary. From the perspective of shape calculus [4, 18] this is a reasonable choice to cover relevant applications. An exemplary computation including geometric constraints can be found in [16]. For the finite setting we recover the general formulation of a problem for the p-Laplacian $\Delta_p v = \nabla \cdot (\|\nabla v\|_2^{p-2} \nabla v)$ reading

$$\arg\min_{u\in\mathscr{U}^p} J_p(u) = \arg\min_{u\in\mathscr{U}^p} \frac{1}{p} \underbrace{\int_\Omega \|\nabla(u+g)\|_2^p \,\mathrm{d}x}_{=:\|u+g\|^p_{X^p(\Omega)}} - \int_\Gamma hu \,\mathrm{d}\Gamma - \int_\Omega fu \,\mathrm{d}x \tag{9.4}$$

over the set $\mathscr{U}^p := \{u \in W^{1,p}(\Omega,\mathbb{R}^d) : u = 0 \text{ a.e. on } \partial\Omega\setminus\Gamma\}$ with $v := u+g$ for an arbitrary extension of g to the whole domain in $\{v \in W^{1,p}(\Omega,\mathbb{R}^d) : v = g \text{ a.e. on } \partial\Omega\setminus\Gamma\}$. The corresponding Euler-Lagrange equation is given by

$$\left.\begin{aligned} -\Delta_p v &= f && \text{in } \Omega,\\ \|\nabla v\|_2^{p-2}\partial_\eta v &= h && \text{on } \Gamma,\\ v &= g && \text{on } \partial\Omega\setminus\Gamma \end{aligned}\right\}.$$

Consequently, in order to obtain an efficient shape optimization algorithm, it is necessary to find an efficient routine to solve this problem for a preferably high order p. On the other hand, it is desirable to directly solve the non-relaxed limit case for $p=\infty$ to obtain analytically valid and possibly superior results.

The remainder is structured as follows: In section 9.2 we construct an algorithm for the vector-valued p-Laplace problem by extending a scalar algorithm and integrating support for Neumann boundary conditions. We present numerical results obtained with this algorithm in section 9.3. After that, we discuss a version of the presented algorithm for $p=\infty$ before we draw conclusions in section 9.5.

9.2 High-Order p-Harmonic Descent

In [11] an algorithm to solve scalar p-Laplace problems with Dirichlet boundary conditions is presented in order to show they are solvable in polynomial time. The approach relies on interior-point methods and the theory of self-concordant barriers, including estimates in terms of the barrier parameter ν given by Nesterov [13]. Besides the computational complexity, one of the main advantages is that the solution to the linear Laplacian is a sufficient initial guess for any p and no iteration over p is required. We construct an extension of the algorithm for vector-valued functions featuring mixed Dirichlet and Neumann boundary conditions in order to apply it to shape deformation problems. However, we will only introduce minor changes to the original proof and show that the polynomial estimate holds with mixed boundary conditions in the scalar setting.

First, we recall some basic notation for finite elements. Let h_Ω be a parameter and T_{h_Ω} a triangulation of Ω with n nodes and m elements. For linear elements, the affine coordinate mapping from the reference element to a physical element K_i can be expressed by $x = J_i r + b_i$. The triangulation is called quasi-uniform if there exists parameter ρ_Ω such that $h_\Omega \le \|J_i\|_2 \le \rho_\Omega h_\Omega$ for all elements. Further let V_{h_Ω} denote the space of vector-valued, piece-wise linear Lagrange elements over T_{h_Ω}.

For a general function $u : \mathbb{R}^d \to \mathbb{R}^{d'}$, the coefficient vector $u \in \mathbb{R}^{nd'}$ is given here by blocks of length d' for each node k. In each of those blocks, all entries are associated with the corresponding classical scalar nodal basis function Φ_k. This allows us to extend the notion of discrete derivative matrices to vector-valued functions by $D^{(j,r)} \in \mathbb{R}^{m \times nd'}$. The entries are given by $D^{(j,r)}_{i,d'(k-1)+r} = \frac{\partial}{\partial x_j}\Phi_k(x^{(i)})$ consisting of derivatives of the basis functions evaluated at the element midpoints $x^{(i)}$. Note that, only the columns that correspond to the respective image dimension r in the block of node k are non-zero. By this construction, the multiplication to a coefficient vector returns the discrete derivative in direction x_j of the r-th image dimension at each element midpoint $x^{(i)}$. Subsequently, the matrices are sparse with entries only in every d'-th column and in these columns only if the node k is in the support of the element i. The vector of weights is given by $\omega^{(l)}$, where l denotes the number of local quadrature points. This also means for triangular elements using the mid-point rule $\omega^{(1)} = \omega$ is the vector of element volumes. The discretization of the p-Laplacian term from the problem (9.4) is then given by

$$\|u+g\|^p_{X^p(\Omega)} = \sum_{i=1}^{m} \omega_i \left(\sum_{j=1}^{d} \sum_{r=1}^{d'} [D^{(j,r)}(u+g)]_i^2 \right)^{\frac{p}{2}}.$$

Further, we define basis matrices $E \in \mathbb{R}^{mld' \times nd'}$ yielding the function value for all image dimensions on the l local quadrature points of all elements on multiplication to a coefficient vector. This discrete operator will later simplify the proof by allowing us apply similar techniques as those for $D^{(j,r)}$ also for the occurring mass matrices $M = [E^{(l)}]^\intercal W^{(l)} E^{(l)}$ where $W^{(l)} = \operatorname{diag}(\omega^{(l)})$.

Note that all definitions hold similarly for boundary elements and will be denoted by a bar, e.g. $\overline{M} = [\overline{E}^{(\bar{l})}]^\intercal \overline{W}^{(\bar{l})} \overline{E}^{(\bar{l})} \in \mathbb{R}^{nd' \times nd'}$.

With these connections established, we can now state the discretized and reformulated problem for the vector-valued p-Laplacian with mixed Dirichlet and Neumann boundary data in the following lemma.

Lemma 9.1. *The problem (9.4) of minimizing $J_p(u)$ over the given finite element space V_{h_Ω} with $1 \le p < \infty$ satisfying the additional upper bound $\omega_i \|\nabla(u+g)|_{K_i}\|_2^p \le R$ is equivalent to the classical convex problem*

$$\underset{x \in \mathscr{Q}_p}{\arg\min} \langle c, x \rangle \text{ with } c = \begin{bmatrix} -Mf - \overline{M}h \\ \frac{\omega}{p} \end{bmatrix} \tag{9.5}$$

with the constrained search set given by

$$\mathscr{Q}_p = \left\{ (u,s) \in \mathbb{R}^n \times \mathbb{R}^m : s_i \ge \left(\sum_{j=1}^{d} \sum_{r=1}^{d'} [D^{(j,r)}(u+g)]_i^2 \right)^{\frac{p}{2}} \wedge \omega_i s_i \le R \right\}. \tag{9.6}$$

The obtained problem is now a classical convex optimization problem by the minimization of a scalar product over a constrained set. An algorithm is obtained by constructing a ν-self-concordant barrier for $\mathcal{Q}_p$, computing its first and second derivative and then applying an interior-point method [13].

Lemma 9.2. *A $4m$-self-concordant barrier for $\mathcal{Q}_p$ is given by the function*

$$F(u,s) = -\sum_i \log z_i - \sum_i \log \tau_i \quad \textit{where}$$

$$z_i = s_i^{2/p} - \sum_{j=1}^{d}\sum_{r=1}^{d'} [(\underbrace{D^{(j,r)}u + D^{(j,r)}g}_{=:y^{(j,r)}})_i]^2 \quad \textit{and} \quad \tau_i = R - \omega_i s_i.$$

Remark 9.1. By construction the barrier function F is twice differentiable with the first derivative reading

$$F' = \begin{bmatrix} F_u \\ F_s \end{bmatrix} \text{ where}$$

$$F_u = 2\sum_{j=1}^{d}\sum_{r=1}^{d'} [D^{(j,r)}]^{\mathsf{T}} \frac{y^{(j,r)}}{z} \quad \text{and} \quad F_s = -\frac{2}{p}\frac{1}{z}s^{2/p-1} + \frac{\omega}{\tau}.$$

The second derivative is given by

$$F'' = \begin{bmatrix} F_{uu} & F_{us} \\ F_{us}^{\mathsf{T}} & F_{ss} \end{bmatrix} \text{ where}$$

$$F_{uu} = 2\sum_{j=1}^{d}\sum_{r=1}^{d'} [D^{(j,r)}]^{\mathsf{T}} Z^{-1} D^{(j,r)} + 4\sum_{j_1=1}^{d}\sum_{r_1=1}^{d'}\sum_{j_2=1}^{d}\sum_{r_2=1}^{d'} (Y^{(j_1,r_1)}D^{(j_1,r_1)})^{\mathsf{T}} Z^{-2} (Y^{(j_2,r_2)}D^{(j_2,r_2)}),$$

$$F_{us} = -\frac{4}{p}\sum_{j=1}^{d}\sum_{r=1}^{d'} (Y^{(j,r)}D^{(j,r)})^{\mathsf{T}} Z^{-2} S^{2/p-1},$$

$$F_{ss} = -\frac{2}{p}\left(\frac{2}{p} - 1\right) Z^{-1} S^{2/p-2} + \frac{4}{p^2} Z^{-2} S^{4/p-2} + W^2 T^{-2},$$

$$S = \operatorname{diag}(s), W = \operatorname{diag}(\omega), Y = \operatorname{diag}(y), Z = \operatorname{diag}(z), T = \operatorname{diag}(\tau).$$

Remark 9.2. Note that in the construction the $\frac{p}{2}$-th power of the norm has been moved. Thus the additional constrained $s_i \geq 0$ would be required, as stated in the original version. However, $z_i \to \infty$ as $s_i \searrow \|\nabla(u+g)|_{K_i}\|_2^2$ or $s_i \nearrow -\|\nabla(u+g)|_{K_i}\|_2^2$ and thus leave us with a correct barrier on the intended set as well additional separated set. Therefore, we drop that condition here and in practice we ensure it by the choice of the initial value with $s_i \geq 0$ and keep track via the line-search in the

adaptive path-following. This not only simplifies the notation, but also reduces the computational effort.

For completeness, we state the proof for the computational complexity in the scalar case with additional Neumann boundary conditions. Note that the obtained bound on the iterations differs from the one in the original version [11, Theo. 1]. This stems from a change we have to introduce to the Hessian and subsequent computations as well as using a different estimate in terms of the barrier parameter, which features $\|c\|^*_{x_F^*}$ instead of $\|\hat{x}\|^*_{x_F^*}$. However, the estimate on the required iterations for a naive interior-point method with fixed step size [13, Sec. 4.2] is only of theoretical interest. Even though the bound is not sharp, the required iterations are not reasonable for practical applications. Therefore, variations with modified step lengths [14] or an adaptive step size control [11] are used. Although estimates are worse in these settings, we will see in section 9.3 that the latter performs significantly better in practice. Consequently, we will not show theoretical results for the vector-valued setting.

Theorem 9.1. *Let $1 \leq p < \infty$. Assume that $\Omega \subset \mathbb{R}^d$ is a Lipschitz polytype of width L and that T_{h_Ω} is a quasi-uniform triangulation of Ω, parametrized by $0 < h_\Omega < 1$ and with quasi-uniformity parameter $1 \leq \rho_\Omega < \infty$. Further assume $g \in W^{1,p}(\Omega)$, $f \in \mathrm{L}^q(\Omega)$ and $h \in \mathrm{L}^q(\Gamma)$ with conjugated exponents $\frac{1}{p} + \frac{1}{q} = 1$ are piece-wise linear on T_{h_Ω} and let $V_{h_\Omega} \subset W_0^{1,p}(\Omega)$ be the piece-wise linear finite element space on T_{h_Ω} whose trace vanishes. Fix a quadrature Q with positive weights such that the integration is exact, $R \geq R^* := 2(1 + \|g\|^p_{X^p(\Omega)})$ sufficiently large and let $\varepsilon > 0$ be an accuracy.*

In exact arithmetic, a naive interior-point method consisting of auxiliary and main path-following using the barrier function from lemma 9.2 to minimize $J_p(u)$ over $u \in V_{h_\Omega}$, starting from $\hat{x} = (0, \hat{s})$ with $\hat{s}_i = 1 + (\sum_j \sum_r [D^{(j,r)} g]_i^2)^{p/2}$, converges to the global minimizer in V_{h_Ω} in at most

$$N \leq 14.4\sqrt{|\Omega| d! h_\Omega^{-d}} \\ [K^* + \log(\varepsilon^{-1} h_\Omega^{-1-7.5d} R^5 (1 + \|g\|_{X^p(\Omega)})(\|f\|_{\mathrm{L}^q(\Omega)} + \|h\|_{\mathrm{L}^q(\Gamma)} + 1))].$$

iterations. This results in a computational complexity denoted by $\mathcal{O}(\sqrt{n}\log(n))$. The constant $K^* = K^*(\Omega, \rho_\Omega, Q)$ depends on the domain Ω, the quasi-uniformity parameter ρ_Ω of the triangulation and the quadrature Q. At convergence, u satisfies

$$J_p(u) \leq \min_{\substack{v \in V_{h_\Omega} \\ \frac{1}{p}\|v+g\|^p_{X^p} \leq R}} J_p(v) + \varepsilon.$$

Proof. In order to compute the final estimate, we need to find a bound for $\|c\|_2$. Let $f \in \mathrm{L}^q(\Omega)$ and $h \in \mathrm{L}^q(\Gamma)$ piece-wise linear such that the quadrature on l points is exact. We can obtain a bound on a similar way as the bound for $\|F'(\hat{x})\|_2$ in the original paper. Start with

$$\|c\|_2 = \left\| \begin{bmatrix} -Mf - \overline{M}h \\ \frac{\omega}{p} \end{bmatrix} \right\|_2 \leq \|Mf\|_2 + \|\overline{M}h\|_2 + \frac{1}{p}\|\omega\|_2.$$

In accordance with the original proof we can bound the first term by

$$\|Mf\|_2 = \|[E^{(l)}]^\intercal W^{(l)} E^{(l)} f\|_2 \leq \|[E^{(l)}]^\intercal W^{(l)}\|_2 \|E^{(l)} f\|_2$$

with the same idea of using $\|[E^{(l)}]^\intercal W^{(l)}\|_2^2 \leq \omega_{\max}^{(l)} \rho([E^{(l)}]^\intercal W^{(l)} E^{(l)})$ and then bounding the spectral radius ρ. This is even easier here, because

$$w^\intercal E^\intercal W E w = \int_\Omega w^2 dx = \|w\|^2_{\mathrm{L}^2(\Omega)} \leq [K'_\Omega]^2 h_\Omega^{2d} \|w\|_2^2$$

can be estimated without further inequalities. The remainder can now be bound correspondingly with the equivalence of p-norms in finite dimensions

$$\begin{aligned} \|Ef\|_2 &\leq [\omega_{\min}^{(l)}]^{-1/2} \left(\sum_{i=1}^{ml} \omega_i^{(l)} [E^{(l)} f]_i^2 \right)^{\frac{1}{2}} \\ &\leq [\omega_{\min}^{(l)}]^{-1/2} (ml)^{1/2} \left(\sum_{i=1}^{ml} \omega_i^{(l)} [E^{(l)} f]_i^q \right)^{\frac{1}{q}} \\ &\leq \left(\frac{\omega_{\min}}{C_Q}\right)^{-1/2} (ml)^{1/2} \|f\|_{\mathrm{L}^q(\Omega)} \end{aligned}$$

where we used that the weights on the reference elements are fixed positive and thus there exists a constant $C_Q > 0$ that only depends on the quadrature Q such that $C_Q^{-1} \omega_{\min} \leq \omega_{\min}^{(l)} \leq \omega_{\min}$. Combing the results, we get

$$\begin{aligned} \|Mf\|_2 &\leq \left(K'_\Omega h_\Omega^d \right) \left(\omega_{\min}^{-1/2} C_Q^{1/2} l^{1/2} m^{1/2} \|f\|_{\mathrm{L}^q(\Omega)} \right) \\ &\leq K_Q K''_\Omega \|f\|_{\mathrm{L}^q(\Omega)}. \end{aligned}$$

A bound for the middle term can be obtained in the same way, just in $(d-1)$ dimensions. Using

$$|\Gamma| = \sum_{i=1}^{\overline{m}} \overline{\omega}_i \geq \overline{m} \overline{\omega}_{\min} \geq \overline{m} \frac{h_\Omega^{d-1}}{(d-1)!} \Leftrightarrow \overline{m} \leq |\Gamma|(d-1)! h_\Omega^{d-1}$$

this reads

$$\begin{aligned}\|\overline{M}h\|_2 &\leq \left(K'_\Omega h_\Omega^{d-1}\right)\left(\overline{\omega}_{\min}^{-1/2}(C_Q\overline{m}\bar{l})^{1/2}\|h\|_{\mathrm{L}^q(\Gamma)}\right)\\ &\leq K_Q K''_\Omega \|h\|_{\mathrm{L}^q(\Gamma)}.\end{aligned}$$

Subsequently, using $\|\omega\|_2 = \left(\sum_{i=1}^m \omega_i^2\right)^{1/2} \leq \sqrt{m}\omega_{\max} \leq \sqrt{m}\frac{(\rho h_\Omega)^d}{d!}$ and $p^{-1} \leq 1$ we are able to obtain a bound in the form

$$\|c\|_2 \leq C^*_\Omega C^*_Q(\|f\|_{\mathrm{L}^q(\Omega)} + \|h\|_{\mathrm{L}^q(\Gamma)} + 1).$$

Together with the previous results from the original proof we can now determine the relevant bounds as:

$$\begin{aligned}\|c\|^*_{x^*_F} \leq \lambda_{\min}^{-1}\|c\|_2 &\leq \left(c'_\Omega R^{-2}h_\Omega^{2d}\right)^{-1}\left(C^*_\Omega C^*_Q(\|f\|_{\mathrm{L}^q(\Omega)} + \|h\|_{\mathrm{L}^q(\Gamma)} + 1)\right)\\ &= [c'_\Omega]^{-1}C^*_\Omega C^*_Q R^2 h_\Omega^{-2d}(\|f\|_{\mathrm{L}^q(\Omega)} + \|h\|_{\mathrm{L}^q(\Gamma)} + 1)\\ \|F'(\hat{x})\|^*_{x^*_F} \leq \lambda_{\min}^{-1}\|F'(\hat{x})\|_2 &\leq \left(c'_\Omega R^{-2}h_\Omega^{2d}\right)^{-1}\left(C^*_\Omega h_\Omega^{-1-1.5d}R(1+\|g\|_{X^p(\Omega)})\right)\\ &= [c'_\Omega]^{-1}C^*_\Omega R^3 h_\Omega^{-1-3.5d}(1+\|g\|_{X^p(\Omega)})\end{aligned}$$

Plugging these into the bound on the required Newton iterations in terms of the barrier parameter ν by Nesterov [13, Sec. 4.2.5]

$$N \leq 7.2\sqrt{\nu}\,[2\ln(\nu) + \ln(\|F'(\hat{x})\|^*_{x^*_F}) + \ln(\|c\|^*_{x^*_F}) + \ln(1/\varepsilon)],$$

we compute a bound in terms of number of grid points as

$$\begin{aligned}N &\leq 7.2\sqrt{4m}[2\log(4m) + \log(1/\varepsilon)\\ &\quad + \log([c'_\Omega]^{-1}C^*_\Omega R^3 h_\Omega^{-1-3.5d}(1+\|g\|_{X^p(\Omega)}))\\ &\quad + \log([c'_\Omega]^{-1}C^*_\Omega C^*_Q R^2 h_\Omega^{-2d}(\|f\|_{\mathrm{L}^q(\Omega)} + \|h\|_{\mathrm{L}^q(\Gamma)} + 1))]\\ &\leq 14.4\sqrt{|\Omega|d!h_\Omega^{-d}}[\log([c'_\Omega]^{-2}[C^*_\Omega]^2 C^*_Q 16|\Omega|^2(d!)^2)]\\ &\quad + \log(\varepsilon^{-1}h_\Omega^{-1-7.5d}R^5(1+\|g\|_{X^p(\Omega)})(\|f\|_{\mathrm{L}^q(\Omega)} + \|h\|_{\mathrm{L}^q(\Gamma)} + 1))]\\ &= 14.4\sqrt{|\Omega|d!h_\Omega^{-d}}[K^*(\Omega,\rho_\Omega,Q)\\ &\quad + \log(\varepsilon^{-1}h_\Omega^{-1-7.5d}R^5(1+\|g\|_{X^p(\Omega)})(\|f\|_{\mathrm{L}^q(\Omega)} + \|h\|_{\mathrm{L}^q(\Gamma)} + 1))].\end{aligned}$$

Using $h_\Omega^{-d} = \mathcal{O}(n)$, we obtain the corresponding complexity estimate by inspection.

Finally, the convergence error is given by substituting J_p into the general formula associated with the iteration bound in terms of the barrier parameter.

□

Remark 9.3. To find the global minimum, R has to be chosen sufficiently large, so that the solution is contained in the search set $\mathcal{Q}_p$. For $2 \leq p < \infty$ such an upper bound exists and is given by

$$R = 2 + 4\|g\|^p_{X^p(\Omega)} + 8(p-1)\left[L^q\|f\|^q_{\mathrm{L}^q(\Omega)} + C_T^q(L^q+1)\|h\|^q_{\mathrm{L}^q(\Gamma)}\right]$$

where C_T denotes the Sobolev trace constant [5], which only depends on p and Ω. While there even exists an uniform upper bound for it [6], usually neither of them is computable. Therefore, in the actual implementation we choose a heuristic approach. Start by dropping the term resulting from the Neumann boundary condition and if the values during the iteration come close to the bound, restart with an increased version.

Proof. We follow the original proof for the pure Dirichlet case, showing an upper bound for a minimizing sequence u_k using Hölder's inequality, the modified Friedrichs inequality for $\|\cdot\|_{X^p(\Omega)}$ and the Sobolev trace theorem for the new term.

Start by assuming $\|u\|_{X^p(\Omega)} \geq \|g\|_{X^p(\Omega)}$, since otherwise the bound is trivial, and compute

$$\begin{aligned}
J(u) &= \frac{1}{p}\|u+g\|^p_{X^p(\Omega)} - \int_\Omega fu\,\mathrm{d}x - \int_\Gamma hu\,\mathrm{d}\Gamma \\
&\geq \frac{1}{p}\left(\|u\|_{X^p(\Omega)} - \|g\|_{X^p(\Omega)}\right)^p - \|f\|_{\mathrm{L}^q(\Omega)}\|u\|_{\mathrm{L}^p(\Omega)} - \|h\|_{\mathrm{L}^q(\Gamma)}\|u\|_{\mathrm{L}^p(\Gamma)} \\
&\geq \frac{1}{p}\|u\|^p_{X^p(\Omega)} - \frac{1}{p}\|g\|^p_{X^p(\Omega)} - \|f\|_{\mathrm{L}^q(\Omega)}Lp^{-\frac{1}{p}}\|u\|^p_{X^p(\Omega)} \\
&\quad - \|h\|_{\mathrm{L}^q(\Gamma)}C_T(Lp^{-\frac{1}{p}}+1)\|u\|^p_{X^p(\Omega)}.
\end{aligned}$$

Now we can modify the application of Young's inequality for two forcing terms to $a_1 = 4^{\frac{1}{p}}Lp^{-\frac{1}{p}}\|f\|_{\mathrm{L}^q(\Omega)}$, $a_2 = 4^{\frac{1}{p}}C_T(Lp^{-\frac{1}{p}}+1)\|h\|_{\mathrm{L}^q(\Gamma)}$ and $b_{1,2} = 4^{-\frac{1}{p}}\|u\|_{X^p(\Omega)}$ and thus get

$$\begin{aligned}
J(u) - J(0) \geq \frac{1}{2p}\|u\|^p_{X^p(\Omega)} - \frac{2}{p}\|g\|^p_{X^p(\Omega)} - \frac{1}{q}\underbrace{4^{\frac{q}{p}}}_{\substack{\leq 4 \\ \text{for } p\geq 2}}\underbrace{p^{-\frac{q}{p}}}_{\leq 1}L^q\|f\|^q_{\mathrm{L}^q(\Omega)} \\
- \frac{1}{q}4^{\frac{q}{p}}C_T^q\underbrace{(Lp^{-\frac{1}{p}}+1)}_{\leq (Lq^{-\frac{q}{p}}+1)}\|h\|^q_{\mathrm{L}^q(\Gamma)}.
\end{aligned}$$

Therefore, if

$$\|u\|^p_{X^p(\Omega)} > 4\|g\|^p_{X^p(\Omega)} + 8(p-1)\left[L^q\|f\|^q_{\mathrm{L}^q(\Omega)} + C_T^q(L^q+1)\|h\|^q_{\mathrm{L}^q(\Gamma)}\right] =: \tilde{R},$$

then $J(u) - J(0) \geq 0$. By contradiction any minimizing sequence u_k must fulfill $\|u_k\|^p_{X^p(\Omega)} \leq \tilde{R}$ for some k large enough. Thus, it is in the set $\mathcal{Q}_p$ and the final bound is obtained by $R := 2(\tilde{R}+1)$ to ensure the construction condition for the initial value. □

9.3 Numerical Results

In this section, we present results for numerical experiments with the scheme presented in section 9.2. The data was calculated with an implementation in julia based on the finite element library MinFEM [17] and visualized with Paraview. We choose julia since it allows straightforward computations using matrix or vector based operations, enables easy adaptation of the code and provides great accessibility to accuracy parameters. The code and the examples presented here are available in an online repository [19] and as the package PLaplace in the julia registry.

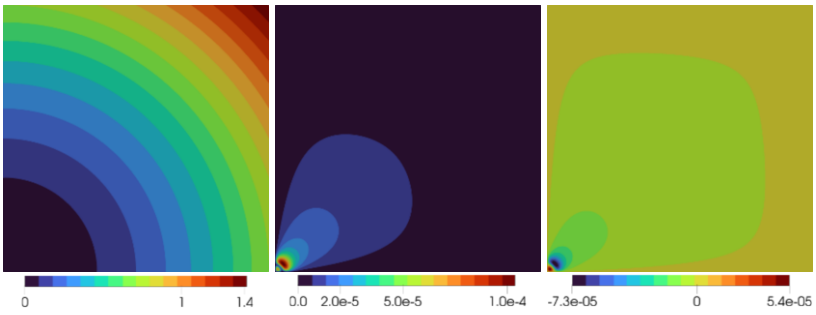

(a) $\|v\|_2$ (b) $\|v - v^*\|_2$ (c) $v_r - v_r^*$

Fig. 9.1: Solution and error for validation by method of manufactured solutions for $v^* = \frac{1}{2}\|x\|_2 \cdot [1,1]^\intercal$ on $\Omega = [0,1]^2$.

We start by validating the algorithm and the implementation. For that purpose, we use the method of manufactured solutions [15] to approximate the analytical solution $v^* = \frac{1}{2}\|x\|_2 \cdot [1,1]^\intercal$ given for the problem

$$\left.\begin{aligned} -\Delta_p v &= -p 2^{\frac{p-2}{2}} \|x\|_2^{p-2} \cdot \begin{bmatrix} 1 \\ 1 \end{bmatrix} && \text{in } \Omega \\ v &= \tfrac{1}{2}\|x\|_2^2 \cdot \begin{bmatrix} 1 \\ 1 \end{bmatrix} && \text{on } \partial\Omega \end{aligned}\right\}.$$

We only test the vector-valued setting, since it contains the scalar case, which has not been validated so far, per component. Figure 9.1 shows the obtained solution and the error on the unit square discretized by a regular mesh with 40000 nodes. The error in the two components is identical and in the order of the intended accuracy $\varepsilon = 10^{-6}$. The largest errors naturally occurs in the bottom left corner, where a function value close to 0 has to be approximated. Thus we consider the results obtained by our implementation as valid.

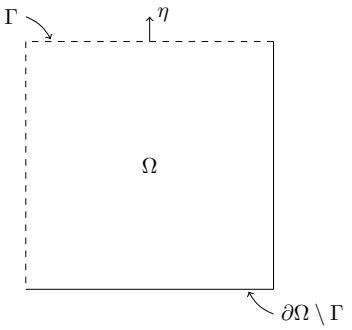

Fig. 9.2: Sketch of domain for exemplary problem.

From now on, we focus on the additional Neumann boundary conditions. Therefore, we consider the domain Ω as the unit square, where left and upper boundary are free for deformation and denoted by Γ. A sketch of this domain can be found in Figure 9.2. On the free boundary, we will work with combinations of the function $\hat{h}(x) = \sin(2\pi x_1) - \sin(2\pi x_2)$. This is a sine wave cycle on each part of the boundary, where the one on the upper boundary is inverted such that the two positive parts are next to the upper left corner. As we will see later, this construction leads towards a distance function on the boundary of the limit solution instead of multiple hats.

$h =$	$\hat{h}(x)$			$\hat{h}(x) \cdot \eta$			$\hat{h}(x) \cdot [1,1]^\intercal$		
$n =$	2500	10000	40000	2500	10000	40000	2500	10000	40000
$p = 2$	95	102	116	94	101	115	95	104	116
$p = 3$	95	104	114	93	101	114	96	107	115
$p = 5$	92	103	113	92	102	107	98	129	116
$p = 8$	118	213	198	86	99	107	186	204	213
$p = 15$	191	253	296	111	126	148	228	278	326
$p = 25$	233	308	464	152	204	181	280	361	481

Table 9.1: Required Newton iterations for solving problems for different boundary source terms with $\hat{h}(x) = \sin(2\pi x_1) - \sin(2\pi x_2)$, number of grid points and PDE parameters p.

For this setting, we can observe the number of required Newton iterations in the path-following with adaptive step-size control for various PDE parameter p and refinements the grid. Table 9.1 shows these values for the scalar setting and two different prolongations of $\hat{h}(x)$ to a vector-valued setting. Note that the vector-valued problems can be a significantly different problem. For example applying $\hat{h}(x)$ to the outer normal vector results in a problem, where per component only one of the free edges features a sine wave and the other one is homogeneous. This is component

wise a simpler problem than the regular scalar one, which is despite the connection of the components visible in the required iterations. The first observation is that much higher orders p are possible when the boundary features a free part. For the pure Dirichlet setting the numerical maximal value was around $p = 5$, here the source term reduces the stiffness of the problem such that even $p = 25$ is possible. In general, we see for all settings the expected behavior of increasing iterations for increasing p and n with some exceptions due to the adaptive stepping. Further, the overall iterations stay comparably small to the number of grid points and thus significantly better than the theoretical estimate. In the scalar Dirichlet case this behavior for the adaptive stepping was already known, but it was unclear if it transfers to the vector-valued setting, especially since the analytical problem is inherently more difficult due to nature of the Frobenius norm in the operator. For the intended application to shape optimization this is a crucial observation, since the computation of many deformation fields is required and thus determines the overall runtime.

Now we will use results obtained for $\hat{h}(x) \cdot \eta$ to calculate the deformation of the square by perturbation of identity (9.1). A selected sequence of transformed domains are shown in Figure 9.3 with a reduced number of grid points for improved visibility. For comparison we take the domain for $p = 2$. This features strong bends near the two fixed endpoints of the free boundary, where the mesh is highly deteriorated. Increasing the order to $p = 5$, the magnitude of the deformation increases significantly and the bends reduce, however the mesh quality is still poor. When changing to $p = 15$, the magnitude changes only slightly as well as the bend. However, the mesh at the bends is not deteriorated anymore and the elements in the interior are deformed more uniformly.

9.4 Descent in $W^{1,\infty}$

In this section, we consider directly solving the steepest descent problem (9.2), commonly associated with the variational problem for the ∞-Laplacian and discuss the challenges arising. The first important property of the ∞-Laplacian is that the solutions are in general non-unique. However, by the approach of regularization with the p-Laplacian, we want the limit of those so-called p-Extensions, which is known as the *absolutely minimizing Lipschitz extension (AMLE)* due to early work by Aronsson [2]. Here, the term "absolutely minimizing" denotes functions $v \in C(\Omega)$ with Lipschitz constant $L_v(V) = L_v(\partial V)$ for all $V \Subset \Omega$.

While the minimization formulation for the problem is common, there is no variational formulation with test functions under the integral [9]. Further, only for zero forcing a reformulation to an Euler-Lagrange equation is possible. With this approach it was shown that unique solutions in the above sense exist for boundary extension problems [8]. This remains true for homogeneous Dirichlet problems with non-negative source terms [7]. Here, the unique limit solution can be split into two

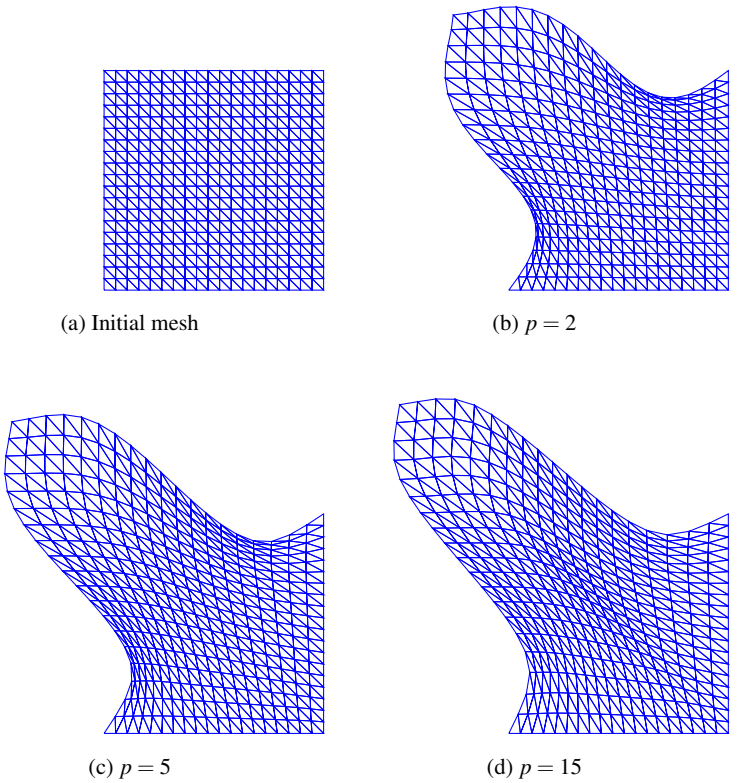

(a) Initial mesh (b) $p = 2$

(c) $p = 5$ (d) $p = 15$

Fig. 9.3: Deformation of a square domain with $h(x) = (\sin(2\pi x_1) - \sin(2\pi x_2)) \cdot \eta$ prescribed on the left and upper boundary for increasing p.

regions. In the support of the source term, the solution is given by the distance to the boundary $\operatorname{dist}(x, \partial\Omega)$. The other region is then given by the unique solution of the ∞-Laplacian without forcing and the distance as Dirichlet boundary condition.

In one dimension, the situation is simplified and analytical solutions can be computed even for source terms with changing sign. Figure 9.4 shows such solutions and corresponding solutions of p-harmonic relaxations for different source terms. We can observe that the limit solution always has slope 1. Its magnitude does not depend on the magnitude of the source term, but only on the length of the interval between two sign changes. However, the p-harmonic solutions depend on it, meaning that the approximation quality depends on the magnitude of the source term as well. Another interesting observation can be made in the lower right plot. The solu-

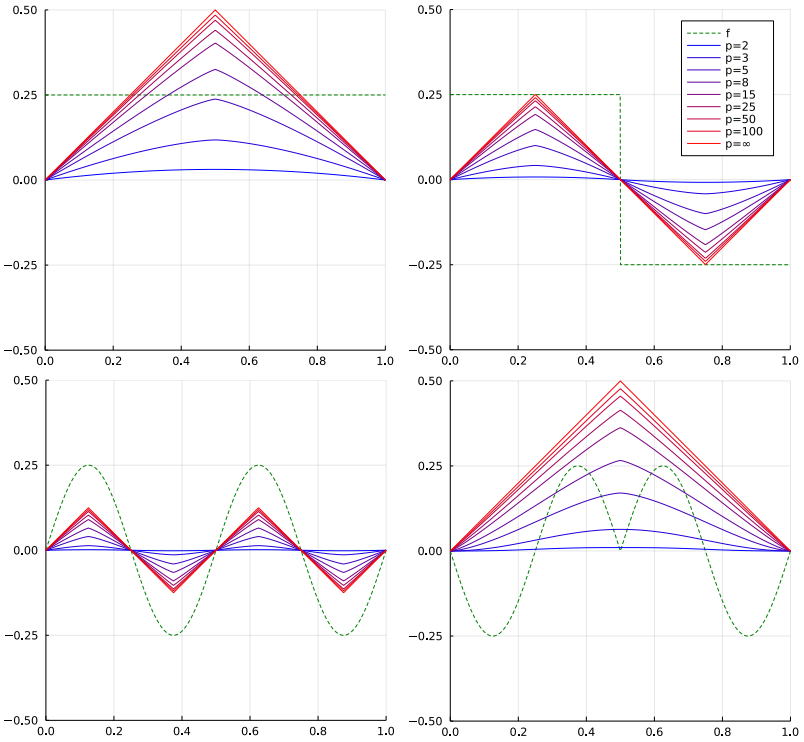

Fig. 9.4: Convergence of numerical solutions for the p-Laplacian with increasing order and the analytical limit $p = \infty$ in $[0,1]$ for $g = 0$ and different source terms f.

tions are able to eliminate certain areas with different signs. While the limit solution is identical to the one with constant source term, the p-harmonic approximations are different. Especially one can still see an impact of the sign change close to the boundary and the kink at tip occurs later. Further, this one dimensional source term is similar to a normalized version of the Neumann boundary condition or boundary source term used in Figure 9.3. Thus, we would expect a solution with slope 1 everywhere on the boundary for the limit deformation.

Additionally to the algorithm for the finite setting, which we modified in section 9.2, an algorithm for the limit problem is proposed in [11]. There, the limit of problem (9.4) is formulated as

$$\arg\min_{u\in\mathscr{U}^\infty} J_\infty(u) = \arg\min_{u\in\mathscr{U}^\infty} \underbrace{\sup_{x\in\Omega} \|\nabla(u+g)\|}_{=:\|u+g\|_{X^\infty(\Omega)}} - \int_\Gamma hu \,\mathrm{d}\Gamma - \int_\Omega fu \,\mathrm{d}x. \tag{9.7}$$

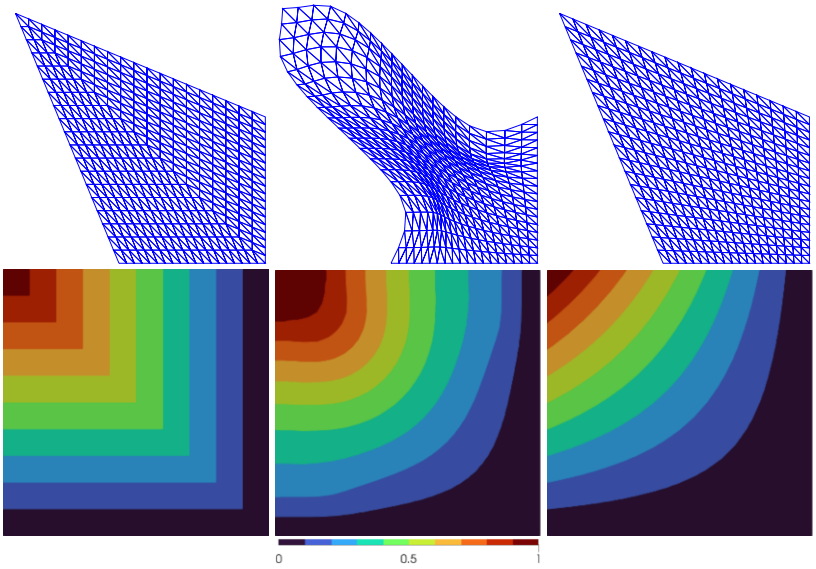

(a) Expected limit. (b) Inner norm $\|\cdot\|_2$. (c) Inner norm $\|\cdot\|_\infty$.

Fig. 9.5: Deformation of a square domain with $h(x) = (\sin(2\pi x_1) - \sin(2\pi x_2)) \cdot \eta$ prescribed on the left and upper boundary for different different algorithmic realizations of the ∞-Laplacian.

First, note that we leave the interpretation of the interior norm in the first term open for now. While there is no actual derivation of the formulation given, we can state some arguments to consider it. Interpreting the primary term in equation (9.4) as $\|u+g\|^p_{X^p(\Omega)}$ one would obtain this primary term as $\|u+g\|_{X^\infty(\Omega)}$ in the same way classical limits for L^p-norms are constructed. By the theory of Lipschitz extensions [8], one can understand the ∞-Laplacian as the minimization of the sup norm of the gradient, given further justification to the idea.

We will not give the construction of the algorithm here again, since it is similar to the finite setting and the extensions are done in the same manner. However, it is interesting that the reformulated discrete problem (9.5) essentially becomes a problem for the 1-Laplacian over the subspace of constant s meaning that the Lipschitz constant on each element is bounded uniformly and the bound is minimized. On the Neumann boundary this approach would result in $v|_\Gamma = 0$ and thus we add the constraint $s \geq 1$ in order to obtain the desired slope on the boundary.

From the sequence of solutions for finite p and the observations in 1D combined with the theoretical definition of the AMLE, we expect the limit artificially shown in Figure 9.5a. Figure 9.5b shows the result for the choice of the inner norm $\|\cdot\|_2$ in equation (9.7) as proposed in [11]. It overshoots the intended tip slightly, yielding

an improvement to the solution for $p = 15$ from Figure 9.3. But it is not able to resolve the intended free boundaries, leading to worse results than the finite setting. However, the grid quality at those boundaries remains good and instead the center becomes significantly worse. By the method of manufactured solutions, we can also show that it is not able to yield the unique solution for a reference problems with the well-known viscosity solution $v = x_1^{4/3} - x_2^{4/3}$ [10]. Another approach is choosing the supremum norm also for the inner norm, which we computed in Figure 9.5c. While this choice yields the correct outer boundary, it still does not deform the interior mesh uniformly.

9.5 Conclusion

We added support for Neumann boundary conditions to a present algorithm for the scalar p-Laplacian and proved that the theoretical estimate on the required Newton steps remains polynomial. Further, we constructed the extension of the algorithm to vector-valued problems and performed numerical experiments including validation and shape deformations. The results demonstrate that the extension is indeed applicable to problems occurring in p-harmonic shape optimization and yields solutions for higher-order $p > 5$ without iterating over p. Those provide further improvements in terms of preserved mesh quality and obtained boundary shape. However, we saw that results obtained for the ∞-Laplacian are significantly different and even high-order solutions do not yield a sufficient approximation, especially since they depend on the magnitude of the source term. First experiments with a modified algorithm to solve the ∞-Laplacian problem directly did not yield the desired results, but small changes could already achieve improvements, allowing the idea to be considered further.

For future research it remains to construct a proper algorithm for the limit problem. On the other hand, the results for finite p may be applied in shape optimization problems potentially including 3D settings. This includes modifications to the implementation for high-performance computer architecture and analysis considering scalability.

Acknowledgment

The authors acknowledge the support by the Deutsche Forschungsgemeinschaft (DFG) within the Research Training Group GRK 2583 “Modeling, Simulation and Optimization of Fluid Dynamic Applications”.

References

1. G. Allaire, C. Dapogny, and F. Jouve. Shape and topology optimization. In: *Geometric Partial Differential Equations - Part II*. *Handbook of Numerical Analysis*, vol. 2, Elsevier, 1–132, 2021.
2. G. Aronsson, M. Crandall, and P. Juutinen. A tour of the theory of absolutely minimizing functions. *Bulletin of The American Mathematical Society* **41**, 2004.
3. K. Deckelnick, P.J. Herbert, and M. Hinze. A novel $W^{1,\infty}$ approach to shape optimisation with Lipschitz domains. *ESAIM: Control, Optimisation and Calculus of Variations* **28**, 2022.
4. M.C. Delfour and J.-P. Zolesio. *Shapes and Geometries: Metrics, Analysis, Differential Calculus, and Optimization*. Advances in Design and Control, vol. 2, SIAM, 2nd edition, 2011.
5. L.C. Evans and R.F. Gariepy. *Measure Theory and Fine Properties of Functions*. Chapman and Hall, revised edition, 2015.
6. J. Fernández Bonder, J. Rossi, and R. Ferreira. Uniform bounds for the best Sobolev trace constant. *Advanced Nonlinear Studies* **3**, 181–192, 2003.
7. H. Ishii and P. Loreti. Limits of solutions of p-Laplace equations as p goes to infinity and related variational problems. *SIAM Journal on Mathematical Analysis* **37**(2), 411–437, 2005.
8. R. Jensen. Uniqueness of Lipschitz extensions: minimizing the sup norm of the gradient. *Archive for Rational Mechanics and Analysis* **123**(1):51–74, 1993.
9. P. Lindqvist. Notes on the p-Laplace Equation. *Report. University of Jyväskylä Department of Mathematics and Statistics*, 102, 2006.
10. P. Lindqvist. *Notes on the Infinity Laplace Equation*. Springer Briefs in Mathematics. Springer International Publishing, 1st edition, 2016.
11. S. Loisel. Efficient algorithms for solving the p-Laplacian in polynomial time. *Numerische Mathematik* **146**(2), 369–400, 2020.
12. P.M. Müller, N. Kühl, M. Siebenborn, K. Deckelnick, M. Hinze, and T. Rung. A novel p-harmonic descent approach applied to fluid dynamic shape optimization. *Struct. Multidic. Optim.* **64**, 2021.
13. Y. Nesterov. *Introductory Lectures on Convex Optimization: A Basic Course*. Applied Optimization, Kluwer Academic Publishers, 2004.
14. Y. Nesterov and A.S. Nemirovskij. *Interior-Point Polynomial Algorithms in Convex Programming*. Studies in Applied Mathematics, SIAM, 2001.
15. K. Salari and P. Knupp. *Code Verification by the Method of Manufactured Solutions*. Sandia Report, 2000.
16. V. Schulz and M. Siebenborn. Computational comparison of surface metrics for PDE constrained shape optimization. *Computational Methods in Applied Mathematics* **16**(3), 485–496, 2016.
17. M. Siebenborn and H. Wyschka. MinFEM. `https://github.com/MinFEM/MinFEM.jl`, 2022.
18. J. Sokolowski and J.-P. Zolesio. *Introduction to Shape Optimization: Shape Sensitivity Analysis*. Springer Series in Computational Mathematics, vol. 16, Springer, 1992.
19. H. Wyschka. PLaplace. `https://github.com/hwyschka/PLaplace.jl`, 2022.